AIP | Applied Physics Letters

Measurement of charge distribution in actin bundles by surface potential microscopy

Peng Zhang and Horacio F. Cantiello

Citation: Appl. Phys. Lett. **95**, 033701 (2009); doi: 10.1063/1.3167281
View online: http://dx.doi.org/10.1063/1.3167281
View Table of Contents: http://apl.aip.org/resource/1/APPLAB/v95/i3
Published by the American Institute of Physics.

Measurement of charge distribution in actin bundles by surface potential microscopy

Peng Zhang and Horacio F. Cantiello[a)]
Nephrology Division and Electrophysiology Core, Massachusetts General Hospital and Harvard Medical School, 149 13th Street, Charlestown, Massachusetts 02129, USA

(Received 25 February 2009; accepted 6 May 2009; published online 21 July 2009)

Bundles of filamentous actin (F-actin) deposited on a gold-plated surface were concurrently imaged using atomic force microscopy (AFM) and surface potential microscopy (SPM). The surface potential was mapped as a function of tip distance to surface using a constant bias potential. There was an uneven spatial distribution of charges detected by SPM, consistent with the segmented topological features shown by AFM of the actin bundles. SPM analysis showed localized changes in surface potential between the axial and transversal sections of the bundles, which are consistent with nonuniform charge distributions of adsorbed salt ions on F-actin. © *2009 American Institute of Physics*. [DOI: 10.1063/1.3167281]

Actin is an abundant cytoskeletal protein in cells. Under physiological conditions, actin polymerizes into filaments (F-actin), which are elongated polymers that behave as highly charged polyelectrolytes.[1–4] Donnan potential measurements of F-actin in solution render higher linear charge densities than theoretically expected.[3] However, charge density is most consistent with a highly uncompensated charge density of actin in solution, which is supported by the coexistence of different electric[1,2] and magnetic[5] dipole moments in F-actin, as well as the ability of F-actin to support ionic condensation-based waves.[6] The above evidence suggests that F-actin contains a fraction of its surrounding counterions in the form of a condensed cloud above its surface. Such a cloud may be highly insensitive to large changes in the ionic strength of the surrounding saline solution,[7–9] and may play an important role in the ability of F-actin to bundle.[4,10] The magnitude and distribution of salt ions on F-actin is, heretofore lacking.

Surface potential microscopy (SPM) is a technique that maps the spatial variation in the potential-energy difference between a tip and a sample, which results from variations in work function.[11,12] Combined with atomic force microscopy (AFM) topological imaging, SPM allows the identification of local charge condensation. The applications of SPM have previously focused on the surface properties of nonbiological materials, particularly semiconductors and metallic surfaces.[13–18] Herein AFM imaging and SPM mapping were concurrently conducted on bundles of F-actin, for the first time to our knowledge. Globular actin (Sigma Chemical Co., St. Louis, MO) was allowed to polymerize at room temperature for at least 12 h in an actin-polymerizing solution containing (in millimole) 100 KCl, 5 $MgCl_2$, 1 adenosine triphosphate, and 10 Hepes [4-(2-hydroxyethyl)-1-piperazineethanesulfonic acid], *p*H 7.4. The solution also contained 1% β-mercaptoethanol. A drop of the F-actin suspension was deposited onto a gold-coated surface (a kind gift of Dr. John Thornton, Veeco Metrology), and F-actin was allowed to settle on the surface for 30 min. The gold-plated surface was then gently washed with distilled H_2O and dried using a flow of N_2. Bundles of F-actin were imaged with a Model 3100 AFM attached to a NanoScope V controller, a kind loan from Veeco Metrology (St. Barbara, CA, see Acknowledgments). Samples were scanned with phosphorus (n) doped Si tips (0.5–2 μm, MESP, Veeco Metrology). The MESP cantilevers have a spring constant (k) of 1–5 N/m, and resonance frequency (f_0) between 60 and 100 kHz. The topological, amplitude, phase and potential signals were simultaneously recorded under TappingMode, at a driving frequency of 90 kHz ($\omega_1 = 2\pi f_0$). Typical scanning areas ranged from 2–20 μm, at a scanning rate of 0.5–1 Hz.

Surface potential measurements (SPM) detect the effective surface voltage of a sample,[11,13,18] such that the feedback mechanism tracks and minimizes the electric force sensed from the sample. SPM can be derived from the energy stored in a parallel capacitor (U):

$$U = \tfrac{1}{2}C(\Delta V)^2, \tag{1}$$

where C is the capacitance between the AFM tip and the sample, and ΔV is the voltage difference between the two. The force at the tip (F) respect to the sample is the rate of energy change with separation distance:[13,18]

$$F = \frac{dU}{dz} = -\frac{1}{2}\frac{dC}{dz}(\Delta V)^2. \tag{2}$$

In our measurements, ΔV consists of both dc (V_{dc}) and ac ($V_{ac} \sin \omega t$) components, where ω is the resonant frequency of the cantilever:

$$\Delta V = \Delta V_{dc} + V_{ac} \sin \omega t. \tag{3}$$

Replacing ΔV in Eq. (2) using Eq. (3) produces the following equation:

$$F = \frac{1}{2}\frac{dC}{dz}\left(\Delta V_{dc}^2 + \frac{1}{2}V_{ac}^2\right) - \frac{dC}{dz}\Delta V_{dc} V_{ac} \sin \omega t + \frac{1}{4}\frac{dC}{dz}V_{ac}^2 \cos(2\omega t). \tag{4}$$

The oscillating electric force acts as a sinusoidal driving force that moves the cantilever. Neither the dc nor 2ω terms contribute to this oscillation. Thus, the amplitude of the electrostatic force, F is given by Eq. (5):

a)Electronic mail: cantiello@helix.mgh.harvard.edu.

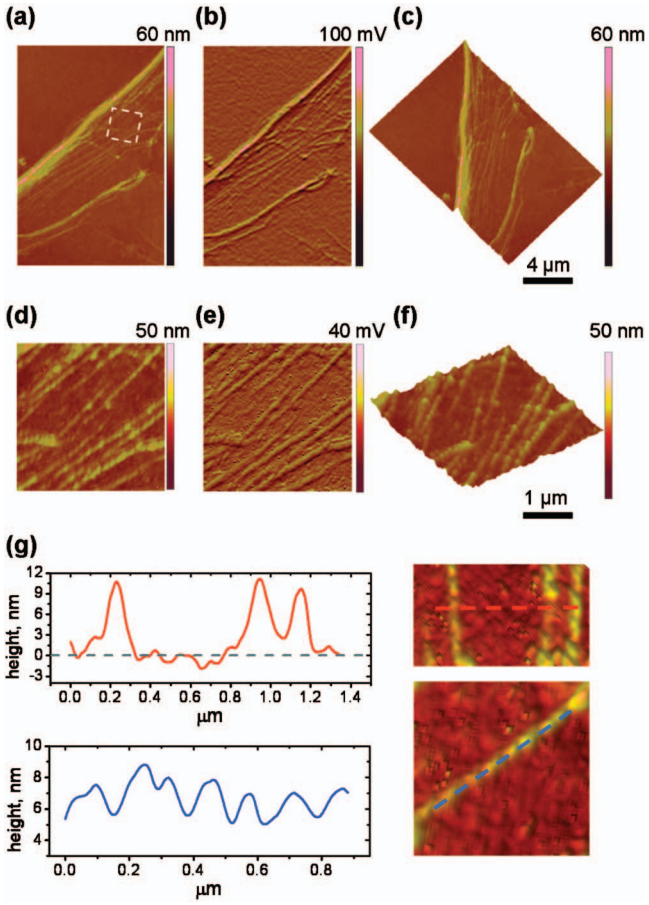

FIG. 1. (Color) AFM images of actin bundles. (a)–(f). Actin bundles spontaneously formed onto a gold-plated surface. Images represent AFM height (left), amplitude (middle) and slanted perspective of the height (right). (d)–(f). Panels are expanded images in (a)–(c), which show the most common bundle sizes. (e) Monomers are evident as distinct round spots in the amplitude scan. (g). Axial (upper) and cross (lower) section histograms of actin bundles shown on the right.

$$F = \frac{dC}{dz}\Delta V_{dc} V_{ac} = \frac{dC}{dz}\Delta V(V_{ac} \sin \omega_2 t). \quad (5)$$

Therefore, changes in the capacitive energy will be a function of dC/dz, which is the derivative of the sample-tip capacitance. The externally applied potential difference between the tip and sample, $\Delta V = V_{tip} - V_{dc}$, is multiplied by the AC component. The dz is the vertical distance between the tip and the sample, and dC is the capacitance between cantilever tip and scanning surface. For the SPM, the scanning angle was 0°, with a scanning capacitance microscopy lock-in phase of −90°, and a constant 4 V voltage (V_{dc}) was applied in tip-biased mode. This was driven by a second frequency-dependent voltage ($V_{ac} \sin \omega_2 t$), where $\omega_2 = 2\pi f_2$, corresponds to a secondary frequency well isolated from mechanical resonance of the microscope head and the cantilever driving frequency used in AFM imaging. AFM images and SPM maps were simultaneously acquired and subsequently analyzed using NANOSCOPE 7.2 software (Veeco Metrology).

AFM imaging showed bundles of F-actin with topological features similar to previously reported.[10,19] Very long filaments were detected [Figs. 1(a)–1(f)], where a bundle type with 106 ± 5.8 nm diameter, and average height of 9.4 ± 0.5 nm was prevalent [Fig. 1(g), upper panels, $n = 14$, the data here and following are all expressed as mean ±SEM]. Actin bundles further assembled to higher-order bundles of larger diameters [Figs. 1(a)–1(c), two thicker bundles of different diameters could be observed]. An axial pattern was also observed with periodic sections with a longitudinal pitch of 148 ± 7.7 nm ($n = 14$) [Figs. 1(d)–1(f)]. This was evidenced by 2.6 ± 0.2 nm ($n = 12$) dimples in the axial topological profile [Fig. 1(g), bottom panels, and Fig. 2(a)], which made the bundles consistent with a packed "string-of-pearls" contour. Surface potential mapping of actin bundles (Fig. 2) was measured as a function of distance (z) of 25–500 nm between the tip and the sample, at a constant bias voltage ($V_{dc} = 4$ V) applied between the tip and the gold surface where the sample was deposited. Surface poten-

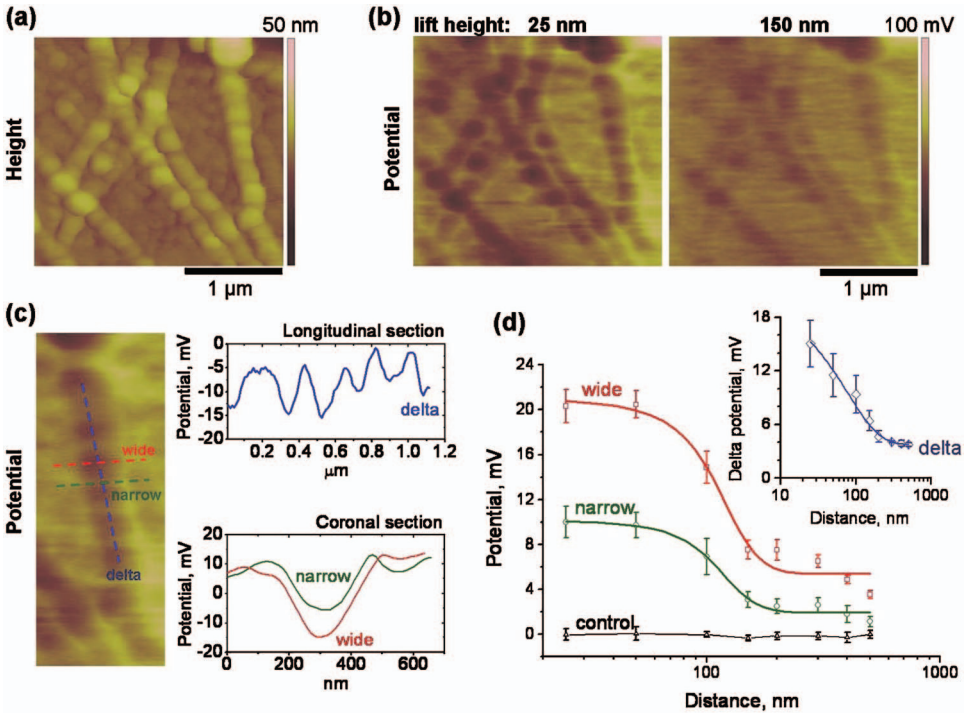

FIG. 2. (Color) SPM scans of actin bundles. (a) Expanded AFM height image of actin bundles chosen for SPM mapping. (b) SPM images of F-actin at two different tip distances indicated on top (25 and 150 nm). (c) SPM mapping of an actin bundle at 25 nm tip distance. Surface potential was obtained for cross sections at wider (red) and narrower (green) diameters, as well as the axial cross section (blue) shown on the right. (d) Surface potential changes as a function of tip distance were determined for wide and narrow cross sections, as well as "control" on the nonactin surface (black). Each point is the average ±SEM of 5–22 measurements from different F-actin segments. Data were fitted to a Boltzmann type profile of V_{tip} (mV) vs z (nm). Inset. The tip potential difference for the axial distribution of dimples follows a single exponential decay function ($n = 3$), with an intercept of 19.6 mV ($z = 0$).

tial (V_{tip}) as a result of a force differential between tip and surface decreased with tip distance [Fig. 2(b)]. It was found that despite the expected inversely proportional relationship of a capacitive component as a function of z (gold surface, control), surface potential saturated as it was closer to the sample [Fig. 2(d)], suggesting a strong nonlinearity in charge distribution. The electrostatic force as a function of distance from the tip in wider and narrower sections of F-actin was best fitted with a Boltzmann-type equation [Fig. 2(d)]:

$$v = \frac{A_1 - A_2}{1 + e^{(z-z_0)/dz}} + A_2, \tag{6}$$

where $A_1 = 21.3$ mV, $A_2 = 5.4$ mV, $z_0 = 110$ nm, and $dz = 25.1$ nm for wider cross section, and $A_1 = 10.3$ mV, $A_2 = 1.9$ mV, $z_0 = 109$ nm, and $dz = 23.8$ nm for narrower cross sections, respectively. In contrast, axial distribution of surface potential differences, as measured by the delta potential (peak and trough) of longitudinal sections was best fitted with a single exponential decay function [Fig. 2(d), inset]:

$$v = A_0 + A \cdot e^{(-z/b)} \tag{7}$$

for the axial distribution of potential differences between the higher and lower heights [Fig. 2(d), insert, where $A_0 = 3.7$ mV, $A = 15.9$ mV, and $b = 77.2$ nm]. This is in agreement with a qualitatively different surface potential in the dimpled constraints of the bundle. The accumulated charge difference in this region (Q), following the relationship $Q = CV^2$, and assuming a $C = 96 \times 10^{-6}$ pF,[20] we can obtain $Q = 2.39 \times 10^{-18}$ C in this region, with excess ions in the order of $15/\text{nm}^3$. Filamentous polyelectrolytes, such as F-actin, have the ability to form a variety of bundles and crosslinked networks. The degree of bundling is affected by ion concentrations in solution.[10,19] Our topological images of F-actin are in agreement with previously reported F-actin thickness.[10] This phenomenon, which is likely due to unbalanced electrostatic interactions, leads to actin bundles with uneven charge distributions. As a result, local variations in surface potential are present in F-actin. The SPM can then be used to detect local distribution of surface charges surrounding polyelectrolytes such as cytoskeletal proteins. The mapping of actin surface potential is consistent with periodically uneven distribution of charges, which may underlie the nonlinear electrical properties of actin.[6] This is particularly evident for those components based on capacitive contributions within actin regions, as well as the uneven interactions between the polymer's surface and excess salt ions adsorbed from the solution. The empirical parameters with which the $V(x)$ profiles were fitted would indicate that the axial distribution of charges follows an exponential decay, while there is apparent saturation when observed from the radial (cross) sections. This suggests different Debye lengths, depending on the direction of the profile. The calculation of numerical solutions for the Debye length is beyond the scope of the present studies. However, a preliminary approximation of the axial profile in our experimental conditions would follow more closely solution(s) to the Poisson equation for $\psi(x)$ such as those observed for the C-V calculations of majority carriers in p-n junctions, accepting that our measurements were not carried out in solution.[21] The difference may suggest, however, that distinct cross sectional profiles are possibly due to the fact that there is a strong interaction with the substrate surface, which has to be further evaluated. In any case, the uncompensated charges spatially extend much longer than the expected Debye length[6] and are thus believed to screen the surface of the polymer such that uneven excess charges might be an essential component to the electrodynamic properties of F-actin.

The authors wish to thank Dean Schmidt, Kim Reed, John Thornton, and Christopher Orsulak from Veeco Metrology (St. Barbara, CA) for lending the Dimension 3100 atomic force microscope coupled to the NanoScope V controller, with which AFM imaging and SPM mapping were made possible.

[1] S. Kobayasi, H. Asai, and F. Oosawa, Biochim. Biophys. Acta **88**, 528 (1964).
[2] S. Kobayasi, Biochim. Biophys. Acta **88**, 541 (1964).
[3] H. F. Cantiello, C. R. Patenaude, and K. S. Zaner, Biophys. J. **59**, 1284 (1991).
[4] J. X. Tang and P. A. Janmey, J. Biol. Chem. **271**, 8556 (1996).
[5] J. Torbet and M. J. Dickens, FEBS Lett. **173**, 403 (1984).
[6] E. Lin and H. F. Cantiello, Biophys. J. **65**, 1371 (1993).
[7] F. Oosawa, Biopolymers **9**, 677 (1970).
[8] G. S. Manning, J. Chem. Phys. **51**, 924 (1969).
[9] B. H. Zimm, in *Coulombic Interactions in Macromolecular Systems*, edited by A. Eisenberg and F. E. Bailey (American Chemical Society, Washington, 1986), p. 212.
[10] K. Shikinaka, H. Kwon, A. Kakugo, H. Furukawa, Y. Osada, J. Gong, Y. Aoyama, H. Nishioka, H. Jinnai, and T. Okajima, Biomacromolecules **9**, 537 (2008).
[11] B. Terris, J. Stern, D. Rugar, and H. Mamin, Phys. Rev. Lett. **63**, 2669 (1989).
[12] M. Nonnenmacher, M. O'Boyle, and H. Wickramasinghe, Appl. Phys. Lett. **58**, 2921 (1991).
[13] R. Nyffenegger and R. Penner, Appl. Phys. Lett. **71**, 1878 (1997).
[14] P. Bridger, Z. Bandic, E. Piquette, and T. McGill, Appl. Phys. Lett. **74**, 3522 (1999).
[15] J. Jones, P. Bridger, O. Marsh, and T. McGill, Appl. Phys. Lett. **75**, 1326 (1999).
[16] Q. Xu and J. Hsu, J. Appl. Phys. **85**, 2465 (1999).
[17] Z. Rakocevic, N. Popovic, Z. Bogdanov, B. Goncic, and S. Strbac, Rev. Sci. Instrum. **79**, 066101 (2008).
[18] S. Shiraishi, K. Kanamura, and Z.-I. Takehara, J. Phys. Chem. B **105**, 123 (2001).
[19] N. Gov, Phys. Rev. E **78**, 011916 (2008).
[20] J. A. Tuszynski, S. Portet, J. M. Dixon, C. Luxford, and H. F. Cantiello, Biophys. J. **86**, 1890 (2004).
[21] W. Johnson and P. Panouysis, IEEE Trans. Electron Devices **18**, 965 (1971).